

DIRECTIONAL DISCRETE COSINE TRANSFORMS ARISING FROM DISCRETE COSINE AND SINE TRANSFORMS FOR DIRECTIONAL BLOCK-WISE IMAGE REPRESENTATION

Tomohiro Ichita¹, Seisuke Kyochi¹, Taizo Suzuki², and Yuichi Tanaka³

1: The University of Kitakyushu, Kitakyushu, Fukuoka, Japan

2: University of Tsukuba, Tsukuba, Ibaraki, Japan

3: Tokyo University of Agriculture and Technology, Koganei, Tokyo, Japan

Email: s-kyochi@kitakyu-u.ac.jp, taizo@cs.tsukuba.ac.jp, ytnk@cc.tuat.ac.jp

ABSTRACT

Directional block transforms (DBTs), such as discrete Fourier transforms, are basically less efficient for sparse image representation than directional overlapped transforms, such as *curvelet* and *contourlet*, but have advantages in practical computation, such as less computational cost, less amount of memory usage to be used, and parallel processing. In order to realize efficient DBTs, this paper proposes directional discrete cosine transforms (DDCTs) by using discrete cosine and sine transforms. The resulting transforms provide richer directional orientations of atoms than conventional DBTs, and thus they are expected to be more efficient for image analysis and processing. In experiments, we evaluate DDCTs with conventional DBTs in image recovery by a convex optimization.

Index Terms— Block transform, discrete cosine transform, directionality, image recovery, convex optimization

1. INTRODUCTION

Sparse image representation (SIR) allows us to analyze images precisely, and realize many image processing tasks, e.g., *denoising*, *deblurring*, and *compressive sensing*, by integrating SIR into convex optimization algorithms [1–3]. For SIR, directional frames have been extensively studied, such as *curvelet* [4], *contourlet* [5], *dirLOT* [6], and *dual-tree complex wavelets/filter banks* [7–11]. Recently, more general systems, so-called *dictionary* [12–14], *non-local frame* [15], and *graph wavelets/filter banks* [16, 17], that explore complex structures or non-local similarity, have been proposed.

Although those transforms can efficiently provide SIR and contribute precise image analysis and processing, they have several problems in practical computation. First, computational complexity is typically high, due to 2D filtering [4–6], sparse coding with iterative scheme [12–14], block matching [15], or large-scale eigenvalue decomposition [16, 17]. Second, they require a large amount of memory usage to store the coefficients. Third, they require global memory access because each support of atoms in those frames is overlapped each other. It disturbs parallel computation.

Block transforms (BTs) are widely used in practical applications, e.g., video coding [18], because supports of atoms are identical or disjoint, and transformation can be parallelized. Moreover, they require low computational cost and a small amount of memory. Conventional directional BTs (DBTs) can be classified into fixed type and adaptive type. The fixed class contains transforms with directionally oriented bases, such as discrete Fourier transform (DFT) and its variants [8, 19, 20]. In the latter class, the adaptive directional transforms apply a BT along predetermined oblique di-

rections [21, 22]. Applications of the latter class are relatively limited because transform directions have to be determined from an image in advance. For example, in image recovery, observed images are usually degraded, and thus suitable directions cannot be easily found. For general purposes, we focus on the former fixed class. The problem on conventional fixed type DBTs is that they contain duplicated atoms in their basis and cannot provide rich directional selectivities¹. This degrades the efficiency of image analysis and processing.

In order to achieve DBTs with rich directional selectivities, we firstly introduce directional discrete cosine transforms (DDCTs), which are constructed from the discrete cosine transform (DCT) and the discrete sine transform (DST). The resulting transform provides richer directionally oriented atoms than conventional DBTs. Then, we extend the DDCT to the biorthogonal DDCTs (BDDCTs) for improving the performance. DCTs and DSTs can be regarded as modulated filter banks [23–25]. By customizing prototype filter coefficients of DCTs and DSTs, we can design higher performance for certain criteria, such as coding gain [26–29], while keeping rich directional selectivity. In the experiments, the DDCT/BDDCT are compared with the conventional DBTs in image inpainting as a practical application and we show their effectiveness.

Notations: Bold-faced lower-case and upper-case letters denote vectors and matrices, respectively. A set of N_r [row] and N_c [column] real-valued matrices is described as $\mathbb{R}^{N_r \times N_c}$. **I**, **J**, and **O** are reserved for the identity, reverse identity and zero matrices, respectively. $\mathbf{A}_{[N]}$ represents an $N \times N$ square matrix. $[\mathbf{x}]_i$ (or x_i) and $[\mathbf{X}]_{i,j}$ (or $X_{i,j}$) denote the i -th element of a vector \mathbf{x} and the (i, j) -th element of a matrix \mathbf{X} , respectively. $\mathbf{X}^{(i,j)} \in \mathbb{R}^{M \times M}$ indicates the (i, j) -th $M \times M$ subblock of $\mathbf{X} \in \mathbb{R}^{ML_1 \times ML_2}$. For a given image $\mathbf{X} \in \mathbb{R}^{N_r \times N_c}$, $\text{vec}(\mathbf{X}) \in \mathbb{R}^{N_r N_c}$ denotes the vectorization of \mathbf{X} , i.e., $x_{N_r j + i} = X_{i,j}$. $\text{bvec}(\mathbf{X}) \in \mathbb{R}^{(ML_1)(ML_2)}$ is the block-wise vectorization of $\mathbf{X} \in \mathbb{R}^{ML_1 \times ML_2}$ as $\text{bvec}(\mathbf{X}) = [\text{vec}(\mathbf{X}^{(0,0)})^\top \text{vec}(\mathbf{X}^{(0,1)})^\top \dots \text{vec}(\mathbf{X}^{(L_1-1, L_2-1)})^\top]^\top$. \otimes denotes the Kronecker product. $\text{diag}(a_0, \dots, a_{M-1})$ and $\text{diag}(\mathbf{A}_0, \dots, \mathbf{A}_{M-1})$ denote diagonal and block diagonal matrices.

2. PRELIMINARIES

2.1. Conventional Block and Directional Block Transforms

DCT (type-II) [30] is one of the most standard transforms and widely used [18]. Its transform matrix $\mathbf{F}_C \in \mathbb{R}^{M \times M}$ is defined as:

$$[\mathbf{F}_C]_{k,n} = \alpha_k \sqrt{\frac{2}{M}} \cos(\theta_{k,n}), \quad \theta_{k,n} = \frac{\pi}{M} k \left(n + \frac{1}{2} \right), \quad (1)$$

¹We use directional selectivity as the number of orientation of atoms.

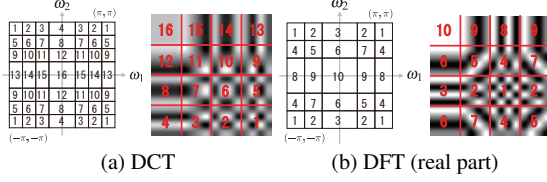


Fig. 1: Frequency partition and the corresponding atoms $\mathbf{B}^{(k_1, k_2)}$ in basis ($M = 4$).

where the ranges of the subband index k and the time index n are $0 \leq n, k \leq M - 1$, $\alpha_0 = \frac{1}{\sqrt{2}}$ ($k = 0$), and $\alpha_k = 1$, ($k \neq 0$). For a block in an image $\mathbf{x} = \text{vec}(\mathbf{X})$ ($\mathbf{X} \in \mathbb{R}^{M \times M}$), the 2D DCT is given by $\mathbf{F}_C \otimes \mathbf{F}_C \in \mathbb{R}^{M^2 \times M^2}$. A drawback of DCT is lack of directional selectivity in its atoms (elements of basis/frames). The 2D atom $\mathbf{B}^{(k_1, k_2)} \in \mathbb{R}^{M \times M}$ in the DCT forms:

$$B_{n_1, n_2}^{(k_1, k_2)} = [\mathbf{F}_C]_{k_1, n_1} [\mathbf{F}_C]_{k_2, n_2} \quad (2)$$

where k_1 and n_1 denote the vertical subband and spatial index, respectively, and k_2 and n_2 denote the horizontal ones ($0 \leq k_1, k_2, n_1, n_2 \leq M - 1$). Clearly, it is not directionally oriented (Fig. 1(a)²), and thus it cannot express various directionally components in images.

The DFT [19] and its variants (discrete Hartley transforms (DHTs) [20] and conjugate-symmetric Hadamard transforms [8]) are the DBTs. For example, the transform matrix of DFT is $[\mathbf{F}_W]_{k, n} = \frac{1}{\sqrt{M}} e^{-j\varphi_{k, n}} \in \mathbb{R}^{M \times M}$ ($\varphi_{k, n} = \frac{2\pi}{M} kn$) and whose 2D atoms $\mathbf{B}^{(k_1, k_2)} \in \mathbb{R}^{M \times M}$ are specified as:

$$B_{n_1, n_2}^{(k_1, k_2)} = \overline{[\mathbf{F}_W]_{k_1, n_1}} [\mathbf{F}_W]_{k_2, n_2} = \frac{1}{M} e^{j(\varphi_{k_1, n_1} + \varphi_{k_2, n_2})}. \quad (3)$$

As shown in Fig. 1(b), the basis contains directionally-oriented atoms. One problem on the DFT and its variants is that they contain duplicated atoms in their basis and cannot provide rich directional selectivity as shown in Fig. 1(b). It means that high efficiency of image analysis and processing cannot be achieved.

2.2. Primal-Dual Splitting Method

Here, we briefly review the primal-dual splitting algorithm (PDS) [31–33] as a solver of a convex optimization problem used in the experiments in Section 4. Consider the following convex optimization problem to find $\mathbf{x}^* \in \arg \min_{\mathbf{x} \in \mathbb{R}^n} g(\mathbf{x}) + h(\mathbf{L}\mathbf{x})$, where $g \in \Gamma_0(\mathbb{R}^n)$, $h \in \Gamma_0(\mathbb{R}^m)$, and $\mathbf{L} \in \mathbb{R}^{m \times n}$. Then the PDS for solving the problem is given as follows:

$$\begin{cases} \mathbf{x}_{k+1} := \text{prox}_{\gamma_1 g}[\mathbf{x}_k - \gamma_1 \mathbf{L}^* \mathbf{z}_k] \\ \mathbf{z}_{k+1} := \text{prox}_{\gamma_2 h^*}[\mathbf{z}_k + \gamma_2 \mathbf{L}(2\mathbf{x}_{k+1} - \mathbf{x}_k)] \end{cases}, \quad (4)$$

where prox denotes the *proximal operator* [34], h^* is the conjugate function [34] of h , and \mathbf{L}^* is the adjoint operator of \mathbf{L} .

3. DISCRETE DIRECTIONAL COSINE TRANSFORM

3.1. Definition of DDCT

In order to solve poor directional selectivity of the conventional DBTs mentioned in Section 2.1, the DDCT is introduced as follows.

²In Figs. 1 and 2, enlarged atoms are depicted for better visualization.

³ $\Gamma_0(\mathbb{R}^N)$ is the set of proper lower semi-continuous convex functions [34] on \mathbb{R}^N .

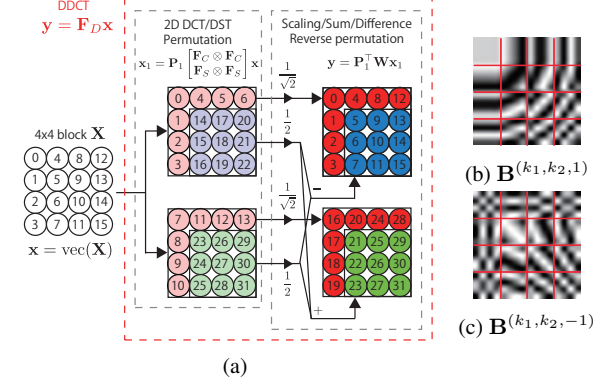


Fig. 2: (a) Procedure of the DDCT ($M = 4$). (b) and (c): Atoms $\mathbf{B}^{(k_1, k_2, \pm 1)}$ in the DDCT frame.

Definition 1. The DDCT $\mathbf{F}_D \in \mathbb{R}^{2M^2 \times M^2}$ is defined as

$$\mathbf{F}_D := \mathbf{P}_1^\top \mathbf{W} \mathbf{P}_1 \begin{bmatrix} \mathbf{F}_C \otimes \mathbf{F}_C \\ \mathbf{F}_S \otimes \mathbf{F}_S \end{bmatrix}$$

$$\mathbf{W} = \begin{bmatrix} \frac{1}{\sqrt{2}} \mathbf{I}_{[2M-1]} & \mathbf{O} & \mathbf{O} \\ \mathbf{O} & \frac{1}{2} \mathbf{I}_{[(M-1)^2]} & -\frac{1}{2} \mathbf{I}_{[(M-1)^2]} \\ \mathbf{O} & \frac{1}{2} \mathbf{I}_{[(M-1)^2]} & \frac{1}{2} \mathbf{I}_{[(M-1)^2]} \end{bmatrix} \quad (5)$$

where \mathbf{F}_C is in (1) and $\mathbf{P}_1 \in \mathbb{R}^{M^2 \times M^2}$ is a permutation matrix. \mathbf{P}_1 places the $4M - 2$ DCT and DST coefficients associated with the subband indices $k_1 = 0$ or $k_2 = 0$ to the first part, and the other $2(M - 1)^2$ coefficients associated with the subband indices $k_1 \neq 0$ and $k_2 \neq 0$ to the last (see Fig. 2(a)). $\mathbf{F}_S \in \mathbb{R}^{M \times M}$ is defined as

$$[\mathbf{F}_S]_{k, n} = \begin{cases} \sqrt{\frac{1}{M}} \sin(\pi(n + \frac{1}{2})) & (k = 0) \\ \sqrt{\frac{2}{M}} \sin(\frac{\pi}{M} k(n + \frac{1}{2})) & (k \neq 0) \end{cases}. \quad (6)$$

\mathbf{F}_S is the row-wise permuted version of the type-II DST. Because the DCT (\mathbf{F}_C) and the DST (\mathbf{F}_S) are orthogonal matrices, the DDCT consists a Parseval frame $\mathbf{F}_D^\top \mathbf{F}_D = \mathbf{I}_{[M^2]}$.

The procedure of the DDCT is illustrated in Fig. 2(a). The DDCT requires just two block transforms, and additions/subtractions between two transforms with scaling operations. Its redundancy ratio is 2, which is the same as the DFT and the DTCWTs [7, 8, 10, 11], and is less redundant than frames and dictionaries, e.g., [13, 14].

According to the above setting, the atoms of the DDCT exhibit rich directional selectivity as explained in the following. Because the DDCT forms a Parseval frame, its atoms are given by $[\mathbf{f}_0 \dots \mathbf{f}_{2M^2-1}] := \mathbf{F}_D^\top$. From (5), each \mathbf{f}_k is 1) an atom in the 2D DCT/DST basis, or 2) an atom arising from the sum/difference of 2D DCT/DST atoms. Let $\mathbf{B}^{(k_1, k_2, 1)}$, $\mathbf{B}^{(k_1, k_2, -1)} \in \mathbb{R}^{M \times M}$ be two directional atoms of the DDCT that correspond to the subband $(k_1, k_2) \in \{1, \dots, M - 1\} \times \{1, \dots, M - 1\}$. They can be represented as

$$\begin{aligned} B_{n_1, n_2}^{(k_1, k_2, \pm 1)} &= [\mathbf{F}_C]_{k_1, n_1} [\mathbf{F}_C]_{k_2, n_2} \pm [\mathbf{F}_S]_{k_1, n_1} [\mathbf{F}_S]_{k_2, n_2} \\ &= \frac{2}{M} \cos(\theta_{k_1, n_1} \mp \theta_{k_2, n_2}). \end{aligned} \quad (7)$$

These 2D cosine functions (this is the reason why \mathbf{F}_D in (5) is termed as DDCT) are lying along various oblique directions, as illustrated in Figs. 2(b) and (c), analogous to the DFT (3).

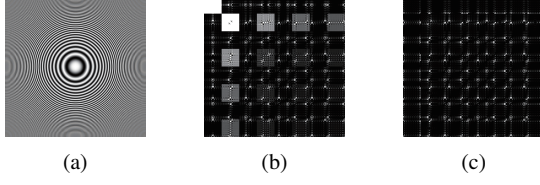


Fig. 3: Frequency responses: (a) *Zoneplate*, (b) (Half of) DDCT coefficients, (c) (Half of) DDCT coefficients using DC shifting.

Whereas the DDCT satisfies the rich directionality, it suffers from DC leakage, as shown in (half of) DDCT coefficients of the input image (*Zoneplate*) in Fig. 3(b). Since DC leakage degrades the energy compaction in the subband domain, we introduce DC shifting as follows. First, let $\mathbf{M} \in \mathbb{R}^{M^2 \times M^2}$ be an averaging operator defined as: $\mathbf{M} = \mathbf{M}_0 \otimes \mathbf{M}_0$, where $\mathbf{M}_0 \in \mathbb{R}^{M \times M}$ and $[\mathbf{M}_0]_{k,n} = \frac{1}{M}$. Then, the transform matrix of the DDCT with DC shifting is defined as $\mathbf{F}_D(\mathbf{I} - \mathbf{M})$. Fig. 3(c) shows the (half of) the transformed coefficients. It is clear that DC shifting ($\mathbf{I} - \mathbf{M}$) can promote sparsity of coefficients.

3.2. Directional Selectivity of DDCT from the Viewpoint of 2D Frequency Domain

Before introducing the BDDCTs, this section discusses the directional selectivity of the DDCT from the viewpoint of 2D frequency domain. Let $H_k^{(c)}(\omega)$ and $H_k^{(s)}(\omega)$ ($k = 1, \dots, M-1$) be the frequency spectrum of the k -th row in DCT and DST, respectively, which can be expressed as

$$\begin{aligned} H_k^{(c)}(\omega) &= \frac{1}{2} \left(U_k(\omega) + \overline{U_k(\omega)} \right) \\ H_k^{(s)}(\omega) &= \frac{1}{2j} \left(U_k(\omega) - \overline{U_k(\omega)} \right), \end{aligned} \quad (8)$$

where $U_k(\omega) = e^{j\frac{\pi}{2M}k} \sum_{n=0}^{M-1} p_{k,n} e^{j(\omega + \frac{\pi}{M}k)n}$, $p_{k,n} = 1$ ($\forall k, n$). While $H_k^{(c)}(\omega)$ and $H_k^{(s)}(\omega)$ distribute in the both positive/negative frequency domain (Fig. 4(a)), $U_k(\omega)$ distributes in the positive frequency domain (Fig. 4(b)). From (8), we can derive

$$\begin{aligned} D_1(\omega_1, \omega_2) &:= \frac{1}{2} \left(U_{k_1}(\omega_1)U_{k_2}(\omega_2) + \overline{U_{k_1}(\omega_1)U_{k_2}(\omega_2)} \right) \\ &= H_{k_1}^{(c)}(\omega_1)H_{k_2}^{(c)}(\omega_2) - H_{k_1}^{(s)}(\omega_1)H_{k_2}^{(s)}(\omega_2) \\ D_2(\omega_1, \omega_2) &:= \frac{1}{2} \left(U_{k_1}(\omega_1)\overline{U_{k_2}(\omega_2)} + \overline{U_{k_1}(\omega_1)}U_{k_2}(\omega_2) \right) \\ &= H_{k_1}^{(c)}(\omega_1)H_{k_2}^{(c)}(\omega_2) + H_{k_1}^{(s)}(\omega_1)H_{k_2}^{(s)}(\omega_2). \end{aligned} \quad (9)$$

As shown the 2D frequency spectra in Figs. 4(c) and (d), (9) ensure that a directional frequency decomposition can be realized by the DDCT (i.e., the 2D separable DCT/DST followed by addition/subtraction).

3.3. Definition of BDDCTs

From (8), DCT and DST can be regarded as special classes of modulated filter banks [23–25]. The fact produces the possibility to enhance the DCT and the DST by finding better prototype lowpass filter coefficients $p_{k,n}$. Now we define biorthogonal DCTs (BDCTs), biorthogonal DSTs (BDSTs), and BDDCTs by extending the original DCT and DST as follows.

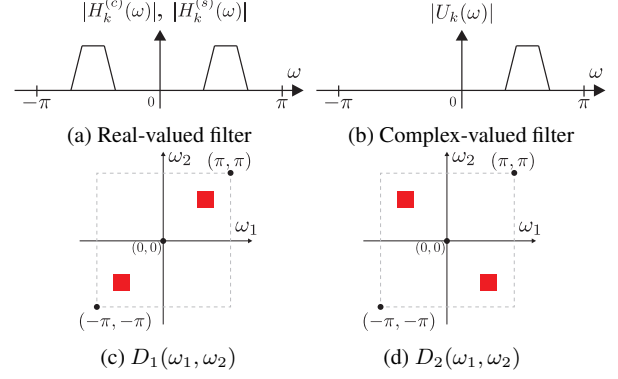


Fig. 4: Example of frequency spectra.

Definition 2. For given coefficients $\{f_n\}_{n=0}^{M-1}$ and $\{g_n\}_{n=0}^{M-1}$, $BDCT \mathbf{F}_{BC} \in \mathbb{R}^{M \times M}$ and $BDST \mathbf{F}_{BS} \in \mathbb{R}^{M \times M}$ are defined as:

$$\begin{aligned} [\mathbf{F}_{BC}]_{k,n} &= p_{k,n} \alpha_k \sqrt{\frac{2}{M}} \cos(\theta_{k,n}) \\ [\mathbf{F}_{BS}]_{k,n} &= p_{k,n} \alpha_k \sqrt{\frac{2}{M}} \sin(\theta_{k,n}) \\ p_{k,n} &= \begin{cases} (f_n + g_n) & k : \text{even} \\ (f_n - g_n) & k : \text{odd} \end{cases}. \end{aligned} \quad (10)$$

BDDCT (denoted as $\mathbf{F}_{BD} \in \mathbb{R}^{2M^2 \times M^2}$) is defined by replacing $DCT \mathbf{F}_C$ and $DST \mathbf{F}_S$ in (5) with $BDCT \mathbf{F}_{BC}$ and $BDST \mathbf{F}_{BS}$.

Since both \mathbf{F}_{BC} and \mathbf{F}_{BS} are often required to be invertible, we should consider the perfect reconstruction condition for BDCTs. For that, we derive the following proposition.

Proposition 1. The matrices \mathbf{F}_{BC} and \mathbf{F}_{BS} can be factorized as:

$$\mathbf{F}_{BC} = \mathbf{F}_C \mathbf{G}_c, \quad \mathbf{F}_{BS} = \mathbf{F}_S \mathbf{G}_s, \quad (11)$$

$$\mathbf{G}_c = \text{diag}(f_0, \dots, f_{M-1}) + \mathbf{J} \text{diag}(g_0, \dots, g_{M-1})$$

$$\mathbf{G}_s = \text{diag}(f_0, \dots, f_{M-1}) - \mathbf{J} \text{diag}(g_0, \dots, g_{M-1})$$

$$\mathbf{G}_s = \mathbf{\Gamma} \mathbf{G}_c \mathbf{\Gamma}, \quad \mathbf{\Gamma} = \text{diag}(\mathbf{I}, -\mathbf{I}). \quad (12)$$

Proof. Due to the symmetry/antisymmetry of the DCT, we obtain

$$\begin{aligned} & \begin{bmatrix} p_{\ell} c_{k,\ell} & p_{M-1-\ell} c_{k,M-1-\ell} \end{bmatrix} \\ &= \begin{bmatrix} (f_{\ell} + g_{\ell}) c_{k,\ell} & (f_{M-1-\ell} + g_{M-1-\ell}) c_{k,\ell} \end{bmatrix} \\ &= \begin{bmatrix} c_{k,\ell} & c_{k,\ell} \end{bmatrix} \begin{bmatrix} f_{\ell} & g_{M-1-\ell} \\ g_{\ell} & f_{M-1-\ell} \end{bmatrix} \\ &= \begin{bmatrix} c_{k,\ell} & c_{k,M-1-\ell} \end{bmatrix} \begin{bmatrix} f_{\ell} & g_{M-1-\ell} \\ g_{\ell} & f_{M-1-\ell} \end{bmatrix} \quad (k : \text{even}) \\ & \begin{bmatrix} p_{\ell} c_{k,\ell} & p_{M-1-\ell} c_{k,M-1-\ell} \end{bmatrix} \\ &= \begin{bmatrix} c_{k,\ell} & -c_{k,\ell} \end{bmatrix} \begin{bmatrix} f_{\ell} & g_{M-1-\ell} \\ g_{\ell} & f_{M-1-\ell} \end{bmatrix} \\ &= \begin{bmatrix} c_{k,\ell} & c_{k,M-1-\ell} \end{bmatrix} \begin{bmatrix} f_{\ell} & g_{M-1-\ell} \\ g_{\ell} & f_{M-1-\ell} \end{bmatrix} \quad (k : \text{odd}). \end{aligned} \quad (13)$$

From the above discussion, we can verify the factorization for the BDCT. In a similar way, the statement on the BDST can be checked. \square

Algorithm 1 Solver for (14)

- 1: set $n = 0$ and choose $\mathbf{x}^{(0)}, \mathbf{z}_1^{(0)}, \mathbf{z}_2^{(0)}, \gamma_1, \gamma_2$.
 - 2: **while** stop criterion is not satisfied **do**
 - 3: $\mathbf{x}^{(n+1)} = \text{prox}_{\gamma_1 \iota_{C_{[0,1]}}}(\mathbf{x}^{(n)} - \gamma_1(\mathbf{F}^\top \mathbf{z}_1^{(n)} + \Phi^\top \mathbf{z}_2^{(n)}))$
 - 4: $\mathbf{t}_1^{(n)} = \mathbf{z}_1^{(n)} + \gamma_2 \mathbf{F}(2\mathbf{x}^{(n+1)} - \mathbf{x}^{(n)})$, $\mathbf{t}_2^{(n)} = \mathbf{z}_2^{(n)} + \gamma_2 \Phi(2\mathbf{x}^{(n+1)} - \mathbf{x}^{(n)})$.
 - 5: $\hat{\mathbf{t}}_1^{(n)} = \text{prox}_{\frac{1}{\gamma_2} \rho \|\cdot\|_1}(\frac{1}{\gamma_2} \mathbf{t}_1^{(n)})$, $\hat{\mathbf{t}}_2^{(n)} = \text{prox}_{\frac{1}{\gamma_2} \iota_{\{\mathbf{v}\}}}(\frac{1}{\gamma_2} \mathbf{t}_2^{(n)})$.
 - 6: $\mathbf{z}_k^{(n+1)} = \mathbf{t}_k^{(n)} - \gamma_2 \hat{\mathbf{t}}_k^{(n)}$ ($k = 1, 2$).
 - 7: $n = n + 1$.
 - 8: **end while**
 - 9: Output $\mathbf{x}^{(n)}$.
-

From the proposition, if \mathbf{G}_c is designed to be non-singular, BDCT \mathbf{F}_{BC} , BDST \mathbf{F}_{BS} , and BDDCT \mathbf{F}_{BD} are invertible.

4. EXPERIMENTAL RESULTS

We evaluated the performance of the DDCT/BDDCT in image inpainting [3], i.e., missing pixel recovery, as a practical application.

First, we explain the detail algorithm used in the experiments. The cost function for image inpainting is formulated as follows.

$$\mathbf{x}^* = \arg \min_{\mathbf{x} \in \mathbb{R}^{N_r N_c}} \rho \|\mathbf{F}\mathbf{x}\|_1 + \iota_{C_{[0,1]}}(\mathbf{x}) + F_v(\Phi \mathbf{x}), \quad (14)$$

where $\rho > 0$, $\mathbf{x} = \text{bvec}(\mathbf{X})$, $\mathbf{X} \in \mathbb{R}^{N_r \times N_c}$, $\mathbf{F} = \mathbf{I}_{[N_r N_c / M^2]} \otimes (\mathbf{F}_{BD}(\mathbf{I} - \mathbf{M}))$ or $\mathbf{F} = \mathbf{I}_{[N_r N_c / M^2]} \otimes (\mathbf{F}_D(\mathbf{I} - \mathbf{M}))$, Φ denotes some degradation process, and $\iota_A(\mathbf{x})$ is the indicator function of a set A . $C_{[0,1]}$ is the set of vectors whose entries are within $[0, 1]$. $F_v \in \Gamma(\mathbb{R}^N)$ is a data fidelity term on the observation \mathbf{v} . Since we simply evaluate the performance of the proposed method in image inpainting, we set the data fidelity term as the $\iota_{\{\mathbf{v}\}}(\mathbf{x})$, where the set of $\{\mathbf{v}\}$ consists of the observation \mathbf{v} . In order to solve (14) by PDS, the functions g and h , and the matrix \mathbf{L} in (4) are set as:

$$g(\mathbf{x}) = \iota_{C_{[0,1]}}(\mathbf{x}), \quad h([\mathbf{z}_1^\top \ \mathbf{z}_2^\top]^\top) = \rho \|\mathbf{z}_1\|_1 + \iota_{\{\mathbf{v}\}}(\mathbf{z}_2),$$

$$\mathbf{z}_1 = \mathbf{F}\mathbf{x}, \quad \mathbf{z}_2 = \Phi \mathbf{x}, \quad \mathbf{L} = [\mathbf{F}^\top \quad \Phi^\top]^\top. \quad (15)$$

Then, a solver of (14) can be described in Algorithm 1⁴. For comparison, we also used ℓ_1 -norm of the coefficients obtained by the DCT, the DFT, and the DHT in (14).

The block size was set to $M = 8$. The parameter \mathbf{G}_c (or \mathbf{G}_s) in (11) for the prototype filter of BDCT/BDST was constructed by SVD-based parameterization [26] and optimized by maximizing the coding gain⁵, which evaluates the energy compaction efficiency, i.e., sparse representation, via subband transform. In optimization, we used MATLAB built-in function “*fminunc*” (the resulting coding gains and frequency responses (DST/BDST) are shown in Table 1 and Figs. 5(a)–(b)). The parameters γ_1 and γ_2 in (4), and ρ in (14) were chosen as 0.01, $\frac{1}{12\gamma_1}$, and 0.5. The stopping criterion for Algorithm 1 as $\|\mathbf{x}^{(n+1)} - \mathbf{x}^{(n)}\|_2 \leq 0.01$. We used test images shown in Figs. 5(c)–(e), and *Zoneplate* (Fig. 3(a)). Each observation consists

⁴For $\mathbf{x} \in \mathbb{R}^N$, $[\text{prox}_{\gamma \|\cdot\|_1}(\mathbf{x})]_i = \text{sign}(x_i) \max\{|x_i| - \gamma, 0\}$ (soft-thresholding), $\text{prox}_{\iota_{C_{[0,1]}}}(\mathbf{x})$ is the clipping operation to $[0, 1]$, and $\text{prox}_{\iota_{\{\mathbf{v}\}}}(\mathbf{x}) = \mathbf{v}$, where $\mathbf{v} \in \mathbb{R}^N$ is an observation.

⁵Since the $2M^2 \times M^2$ BDDCT is a 2D oversampled filterbank, we used the generalized coding gain [27] for 2D signals whose normalized autocorrelation is given by isotropic model [28, 29] with the correlation coefficient of 0.95.

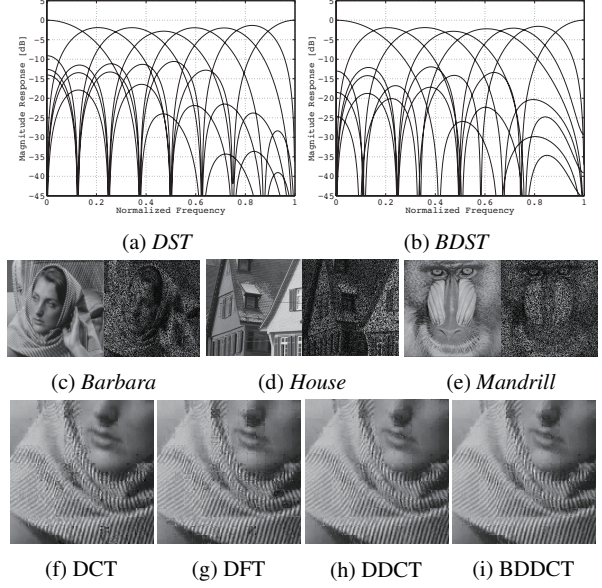


Fig. 5: (a), (b): Frequency responses of DST/BDST, (c)–(e): Original images (256×256) and degraded images (losing 50% pixels), (f)–(i): The (zoomed) resulting images ((h), (i): prop.).

Table 1: (Upper table) Coding gains of DDCT and BDDCT. (Lower table) Numerical results of image recovery.

DDCT ($M = 8$)					BDDCT ($M = 8$)				
11.93					12.52				
<i>Barbara</i> (PSNR [dB]: 9.255)					<i>House</i> (PSNR [dB]: 9.366)				
DCT	DFT	DHT	DDCT	BDDCT	DCT	DFT	DHT	DDCT	BDDCT
25.56	25.33	24.60	26.28	26.65	24.72	24.80	24.16	25.10	25.39
<i>Mandrill</i> (PSNR [dB]: 8.540)					<i>Zoneplate</i> (PSNR [dB]: 7.265)				
DCT	DFT	DHT	DDCT	BDDCT	DCT	DFT	DHT	DDCT	BDDCT
25.13	25.40	24.77	26.10	26.25	14.80	16.41	15.53	17.34	18.31

50% pixels chosen randomly. The matrix Φ in (14) can be obtained by replacing some 1s of an identity matrix to 0 at the indices where corresponding pixels are lost.

Table 1 and Figs. 5(f)–(i) show the experimental results. The BDDCT and the DDCT provided better subjective quality for directional textures than the DCT and the DFT. Although the subjective quality between the BDDCT and the DDCT was almost the same, the BDDCT outperformed the DDCT (and conventional DBTs) in terms of the reconstruction errors (PSNR) because it was optimized to have higher coding gain than that of the DDCT.

5. CONCLUDING REMARKS

In this paper, we proposed the DDCT and the BDDCT. The DDCT was constructed by using DCT/DST and could provide richer directional orientations than conventional DBTs under the same block size. Then, since the DCT and the DST could be regarded as special realizations of modulated filter banks, we could realize the BDDCT that improves the performance of the DDCT by optimizing coefficients in the prototype filter, while keeping the directional selectivity of atoms. In the experimental results, for images with fine textures, the DDCT and BDDCT could achieve higher subjective and numerical qualities than the conventional DBTs.

6. REFERENCES

- [1] P. L. Combettes and J.-C. Pesquet, "A proximal decomposition method for solving convex variational inverse problems," *Inverse Problems*, vol. 24, no. 6, pp. 065014, Nov. 2008.
- [2] N. Pustelnik, C. Chaux, and J. Pesquet, "Parallel proximal algorithm for image restoration using hybrid regularization," *IEEE Trans. Image Process.*, vol. 20, no. 9, pp. 2450–2462, Sep. 2011.
- [3] M. V. Afonso, J. M. B.-Dias, and M. A. T. Figueiredo, "An augmented lagrangian approach to the constrained optimization formulation of imaging inverse problems," *IEEE Trans. Image Process.*, vol. 20, no. 3, pp. 681–695, Mar. 2011.
- [4] J. L. Starck, E. J. Candès, and D. L. Donoho, "The curvelet transform for image denoising," *IEEE Trans. Image Process.*, vol. 11, no. 6, pp. 670–684, June 2002.
- [5] M. N. Do and M. Vetterli, "The contourlet transform: An efficient directional multiresolution image representation," *IEEE Trans. Image Process.*, vol. 14, no. 12, pp. 2091–2106, Dec. 2005.
- [6] C. Zhiyu and S. Muramatsu, "Poisson denoising with multiple directional LOTs," in *Proc. IEEE ICASSP*, Florence, Italy, May 2014, pp. 1225–1229.
- [7] I. W. Selesnick, R. G. Baraniuk, and N. C. Kingsbury, "The dual-tree complex wavelet transform," *IEEE Signal Process. Mag.*, vol. 22, no. 6, pp. 123–151, Nov. 2005.
- [8] S. Kyochi and Y. Tanaka, "General factorization of conjugate-symmetric Hadamard transforms," *IEEE Trans. Signal Process.*, vol. 62, no. 13, pp. 3379–3392, July 2014.
- [9] L. Liang and H. Liu, "Dual-tree cosine-modulated filter bank with linear-phase individual filters: An alternative shift-invariant and directional-selective transform," *IEEE Trans. Image Process.*, vol. 22, no. 12, pp. 5168–5180, Dec. 2013.
- [10] S. Kyochi and M. Ikehara, "A class of near shift-invariant and orientation-selective transform based on delay-less oversampled even-stacked cosine-modulated filter banks," *IEICE Trans. Fundam.*, vol. 93, no. 4, pp. 724–733, Apr. 2010.
- [11] S. Kyochi, T. Uto, and M. Ikehara, "Dual-tree complex wavelet transform arising from cosine-sine modulated filter banks," in *Proc. IEEE ISCAS*, Taipei, Taiwan, May 2009, pp. 2189–2192.
- [12] M. Elad and M. Aharon, "Image denoising via sparse and redundant representations over learned dictionaries," *IEEE Trans. Image Process.*, vol. 15, no. 12, pp. 3736–3745, Dec. 2006.
- [13] M. Aharon, M. Elad, and A. Bruckstein, "K-SVD: An algorithm for designing overcomplete dictionaries for sparse representation," *IEEE Trans. Signal Process.*, vol. 54, no. 11, pp. 4311–4322, Nov. 2006.
- [14] R. Rubinstein, T. Peleg, and M. Elad, "Analysis K-SVD: A dictionary-learning algorithm for the analysis sparse model," *IEEE Trans. Signal Process.*, vol. 61, no. 3, pp. 661–677, Feb. 2013.
- [15] A. Danielyan, V. Katkovnik, and K. Egiazarian, "BM3D frames and variational image deblurring," *IEEE Trans. Image Process.*, vol. 21, no. 4, pp. 1715–1728, Apr. 2012.
- [16] Y. Tanaka and A. Sakiyama, " M -channel oversampled graph filter banks," *IEEE Trans. Signal Process.*, vol. 62, no. 14, pp. 3578–3590, July 2014.
- [17] A. Sakiyama, K. Watanabe, and Y. Tanaka, "Spectral graph wavelets and filter banks with low approximation error," *IEEE Trans. Signal and Inform. Process. Netw.*, vol. 2, no. 3, pp. 230–245, Sep. 2016.
- [18] G. J. Sullivan, J. R. Ohm, W. J. Han, and T. Wiegand, "Overview of the high efficiency video coding (HEVC) standard," *IEEE Trans. Circuits and Syst. for Video Technol.*, vol. 22, no. 12, pp. 1649–1668, Dec. 2012.
- [19] J. W. Cooley and J. W. Tukey, "An algorithm for the machine calculation of complex Fourier series," *Mathematics of Computation*, vol. 19, pp. 297–301, Apr. 1965.
- [20] R. N. Bracewell, "The fast Hartley transform," *Proc. of the IEEE*, vol. 72, no. 8, pp. 1010–1018, Aug. 1984.
- [21] H. Xu, J. Xu, and F. Wu, "Lifting-based directional DCT-like transform for image coding," *IEEE Trans. Circuits and Syst. for Video Technol.*, vol. 17, no. 10, pp. 1325–1335, Oct. 2007.
- [22] B. Zeng and J. Fu, "Directional discrete cosine transforms-A new framework for image coding," *IEEE Trans. Circuits and Syst. for Video Technol.*, vol. 18, no. 3, pp. 305–313, Mar. 2008.
- [23] R. D. Koilpillai and P. P. Vaidyanathan, "Cosine-modulated FIR filter banks satisfying perfect reconstruction," *IEEE Trans. Signal Process.*, vol. 40, no. 4, pp. 770–783, Apr. 1992.
- [24] P. N. Heller, T. Karp, and T. Q. Nguyen, "A general formulation of modulated filter banks," *IEEE Trans. Signal Process.*, vol. 47, no. 4, pp. 986–1002, Apr. 1999.
- [25] G. Doblinger, "A fast design method for perfect-reconstruction uniform cosine-modulated filter banks," *IEEE Trans. Signal Process.*, vol. 60, no. 12, pp. 6693–6697, Dec. 2012.
- [26] T. Suzuki, M. Ikehara, and T. Q. Nguyen, "Generalized block-lifting factorization of M -channel biorthogonal filter banks for lossy-to-lossless image coding," *IEEE Trans. Image Process.*, vol. 21, no. 7, pp. 3220–3228, July 2012.
- [27] T. Tanaka and Y. Yamashita, "The generalized lapped pseudo-biorthogonal transform: Oversampled linear-phase perfect reconstruction filterbanks with lattice structures," *IEEE Trans. Signal Process.*, vol. 52, no. 2, pp. 434–446, Feb. 2004.
- [28] Y. Chen, M. D. Adams, and W.-S. Lu, "Design of optimal quincunx filter banks for image coding," *EURASIP J. Appl. Signal Process.*, vol. 2007, no. 1, pp. 147–147, Jan. 2007.
- [29] M. D. Adams and D. Xu, "Optimal design of high-performance separable wavelet filter banks for image coding," *Signal Processing*, vol. 90, no. 1, pp. 180–196, Jan. 2010.
- [30] K. R. Rao and P. Yip, *Discrete Cosine Transform: Algorithms, Advantages, Applications*, Academic Press Professional, Inc., San Diego, CA, USA, 1990.
- [31] A. Chambolle and T. Pock, "A first-order primal-dual algorithm for convex problems with applications to imaging," *J. Math. Imag. Vis.*, vol. 40, no. 1, pp. 120–145, Dec. 2010.
- [32] L. Condat, "A primal-dual splitting method for convex optimization involving lipschitzian, proximable and linear composite terms," *Journal of Optimization Theory and Applications*, vol. 158, no. 2, pp. 460–479, Aug. 2013.
- [33] B. C. Vu, "A splitting algorithm for dual monotone inclusions involving cocoercive operators," *Adv. Comput. Math.*, vol. 38, no. 3, pp. 667–681, Nov. 2011.
- [34] H. H. Bauschke and P. L. Combettes, *Convex Analysis and Monotone Operator Theory in Hilbert Spaces*, New York, NY, USA: Springer-Verlag, 2011.